Chemical and Morphological Analysis of Surface Enrichment in a Biodegradable Polymer Blend by Phase-Detection Imaging Atomic Force Microscopy

X. Chen, S. L. McGurk, M. C. Davies,* C. J. Roberts,* K. M. Shakesheff, S. J. B. Tendler,* and P. M. Williams

Laboratory of Biophysics and Surface Analysis, School of Pharmaceutical Sciences, The University of Nottingham, Nottingham NG7 2RD, U.K.

J. Davies and A. C. Dawkes

Ortho Clinical Diagnostics, Pollards Wood Laboratories, Nightingales Lane, Chalfont St. Giles, Buckinghamshire HP8 4SP, U.K.

A. Domb

The School of Pharmacy, Faculty of Medicine, The Hebrew University of Jerusalem, Jerusalem, Israel 91120

Received April 3, 1997; Revised Manuscript Received December 15, 1997

ABSTRACT: Surface enrichment phenomena are important in determining the surface organization of fabricated biomaterials and other polymeric materials. Enrichment can govern both the surface chemistry and morphology of such surfaces. Here, we present new information on the surface enrichment of components from a biodegradable polymer blend composed of poly(sebacic anhydride) (PSA) and poly(DL-lactic acid) (PLA). This information, derived by phase-detection imaging atomic force microscopy (AFM), defines both the surface chemistry and morphology. We demonstrate that phase-detection imaging can distinguish between microdomains of PSA and PLA in blends of these biodegradable polymers. Contrast between these two polymers is achieved even when the microdomains cannot be distinguished on surface topography images. The relationship between the force of tapping of the AFM probe on the polymer surface and the image contrast mechanism is investigated. In addition to detecting chemical and mechanical variations on polymer blend surfaces, phase-detection imaging can improve the resolution and contrast of images on single-component films. This is demonstrated by the identification of lamellae with widths of less than 5 nm within PSA spherulites.

Introduction

The surface chemistry and morphology of polymeric biomaterials is the major determinant of the interactions that occur between the polymers and the living environment.[1−3] The important role of this surface organization in biomaterial functioning has encouraged the development of new fabrication techniques that control surface chemistry and morphology.[3−5] One approach to this control is to utilize the inherent surface enrichment of one component of a multicomponent system. Surface enrichment processes have been described as methods of surface engineering for a large number of polymeric materials.[6−8]

The success of surface enrichment as a method of engineering polymer surfaces is dependent on accurate analysis of the final surface organization. The surface chemistry of enriched systems has been quantitatively analyzed using X-ray photoelectron spectroscopy (XPS).[8] Contact angle analysis and static secondary ion mass spectrometry (SSIMS) have also proven beneficial in this characterization.[9−11] While XPS and SSIMS can be used to image surfaces, the resolution of both techniques is insufficient to allow the spatial organization (morphology) of components on enriched surfaces to be visualized on the nanometer-length scale. The characterization of this spatial organization can be performed by microscopy techniques including scanning electron microscopy and scanning probe microscopy. However, in general these techniques have defined the influence of surface enrichment on surface morphology only where it generates significant topographical changes between domains.[12]

Previously, we have described the surface analysis of a biodegradable polymer blend composed of poly(sebacic anhydride) (PSA) and poly(DL-lactic acid) (PLA).[12] These polymers are used to control the rate of drug release from drug delivery systems, the rate being principally controlled by the rate of polymer erosion.[13,14] The hydrolytic lability of the anhydride bond ensures that PSA degrades more rapidly than PLA. Therefore, the degradation kinetics of blends of these two polymers can be controlled by varying the PSA/PLA ratios. However, we have demonstrated by XPS and SSIMS analysis that PLA enriches blend surfaces, resulting in the slower degrading component protecting the PSA. Atomic force microscopy (AFM) analysis of the changes in surface topography during surface erosion confirmed the influence of the surface enrichment of PLA on erosion kinetics. No topographical change occurred to a blend composed of 30% PSA/70% PLA over a 3-h period in a pH 12.5 aqueous solution.

In this paper, we describe an advance in the surface analysis of the PSA/PLA blend system in which phase-detection imaging AFM is used to characterize both the

* To whom correspondence should be addressed. Tel.: + 44 115 951 5063. Fax: + 44 115 951 5110.

S0024-9297(97)00452-X CCC: $15.00
Published on Web 03/15/1998

surface chemical and morphological organization.[15−17] This technique provides new information on the surface organization of this blend because it is possible to visualize regions of the surface that have been enriched with the PLA component, even when this enrichment creates no identifiable topographical feature. The technique is applicable to the study of many other surface enrichment processes used in polymer fabrications. Previously, phase-related contrast has been reported on polystyrene/poly(vinyl methyl ether) blends,[18,19] polyethylene/poly(dimethylsiloxane) blends,[20] and poly(methyl methacrylate)-*block*-polybutadiene-*block*-poly(methyl methacrylate) triblock copolymer.[21] Phase imaging has also been employed to identify individual polystyrene molecules[22] and the components of heterogeneous catalysts made up of radiation-induced metal clusters associated with polymer matrixes.[23]

Methods

Poly(DL-lactic acid) (M_w 50 000) was obtained from Polysciences Inc. (Warrington, U.K.). Poly(sebacic anhydride) (M_w 26 000) was synthesized by a melt condensation polymerization.[24] Samples for AFM analysis were prepared by dissolving 10 mg of polymer in 1 mL of chloroform and then spin casting, at 2000 rpm, a 50-μL aliquot of the polymer solution onto mica or silicon substrates (1 cm × 1 cm squares). The samples were dried under laboratory conditions (approximately 22 °C) for 1 h before analysis. Films were generated with bulk compositions of 80% PSA/20% PLA, 70% PSA/30% PLA, 60% PSA/40% PLA, and 50% PSA/50% PLA. For all samples, the total weight of polymer, dissolved in 1 mL of chloroform, was 10 mg.

AFM was performed with a Multimode NanoScope IIIa (Digital Instruments, Santa Barbara, CA). Tapping mode was employed in air at the cantilever's resonant frequency using a probe and cantilever unit composed of silicon (Nanoprobe, cantilever length 125 μm and resonance frequency 307−375 kHz). Scan rates on all images were 2 Hz. The drive vibration amplitude was 15−45 mV, generating a free cantilever vibration amplitude of 1 V. On a homogeneous surface, the value of cantilever vibration amplitude reduction determines the force with which the probe apex hits the surface. This amplitude reduction can be quantified as the ratio of the setpoint amplitude (A_s) to the free amplitude (A_0). In this paper, we employ two different amplitude reduction ranges of approximately $A_s/A_0 \geq 0.9$ and $0.4 \geq A_s/A_0 \geq 0.2$. When employing the $A_s/A_0 \geq 0.9$ value, the cantilever vibration amplitude is reduced by up to 10% and the probe apex hits the surface relatively softly. For this paper, we define this as soft tapping mode. When employing the $0.4 \geq A_s/A_0 \geq 0.2$ amplitude reduction range, the probe hits the surface harder, we define imaging with these parameters as moderate tapping mode (in-line with similar definitions by Magonov et al.[17]).

To record a phase image, the phase lag of the cantilever vibration compared to the *z*-piezo drive voltage is monitored as the probe scans the surface with a preset constant amplitude of vibration. The phase data contain additional information about the tip−sample interactions resulting from adhesion,[25] surface stiffness,[17] and viscoelastic effects.[26] Maximum height changes and phase shifts for each image are quoted in the corresponding figure captions.

Phase-distance and amplitude-distance curves were recorded by monitoring the phase shift and cantilever oscillation amplitude while taking the tip from a noncontact *z*-position with respect to the sample into contact. Similar dynamic force data have been modeled and obtained by Krüger et al.[27]

Results and Discussion

In our previous studies of PSA/PLA blend surface morphology, using glass as a substrate for thin polymer films, we have observed that the phase separation of the polymer creates micron-scale domains that are identifiable by their characteristic surface topographies.[12] In Figure 1a, we present AFM data from a 90% PSA/10% PLA blend in which topographical data from the AFM is unable to identify PLA regions. The topography shown in these data is dominated by surface-confined spherulites of the semicrystalline PSA component. In Figure 1b, the phase-detection imaging AFM data for this surface region are displayed. These data clearly define a two-component system with a large number of amorphous features overlying the PSA spherulites. The image contrast that allows these amorphous regions to appear as lighter pixels on the AFM data is generated by an increase in the phase shift of +45° over the darker regions of the surface data. Given the known surface enrichment of PLA in these blends and the semicrystallinity of the PSA material, we interpret these data as showing that thin overlayers of PLA cover approximately 50% of the surface of this blend.

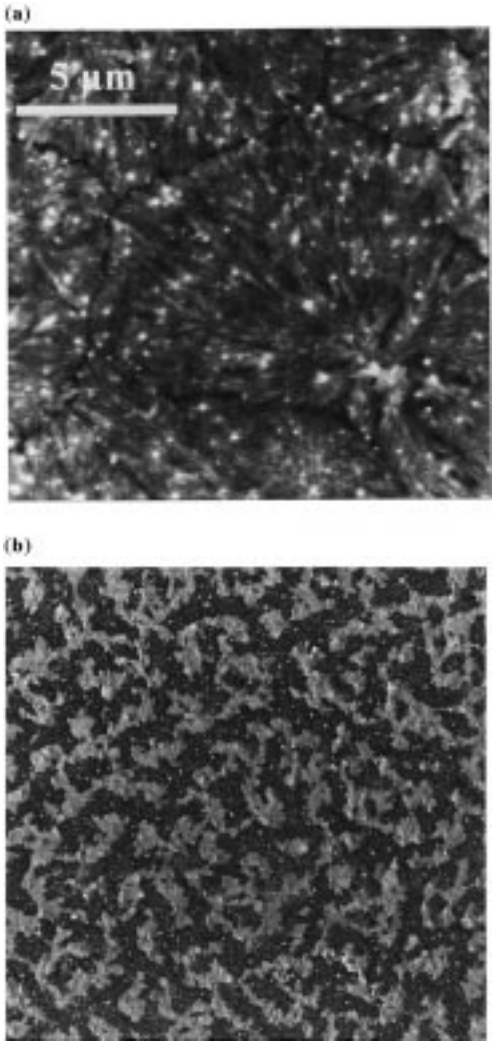

Figure 1. Comparison of amplitude and phase-detection imaging of blends with bulk compositions of 10% PSA/90% PLA: (a) Amplitude-detection imaging of 10% PSA/90% PLA. Height changes 60 nm. (b) Phase-detection imaging of 10% PSA/90% PLA. Maximum phase shift 45°.

Evidence to support our hypothesis that the regions of the surface generating +45° phase shifts are composed of PLA is provided by the analysis of 60% PSA/40% PLA blends. An example of the amplitude-detection and phase-detection imaging AFM data for

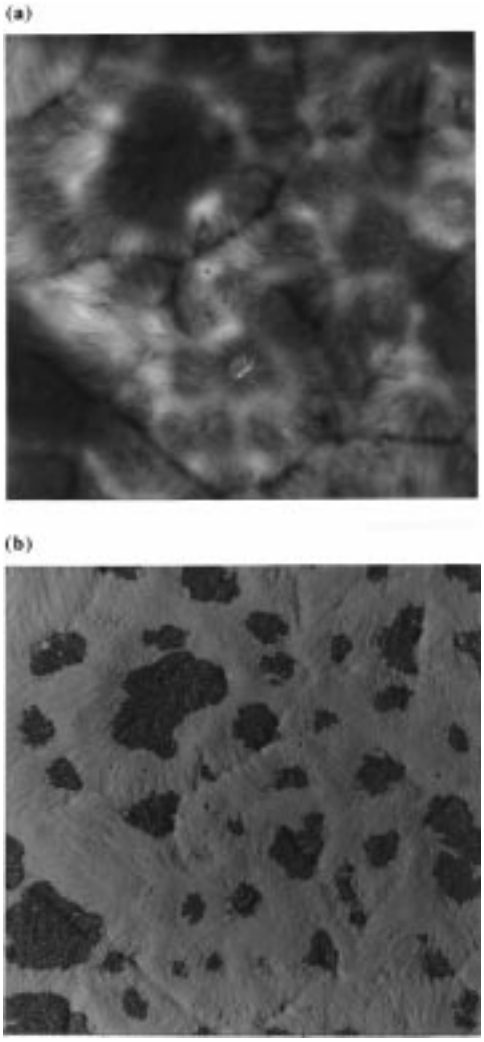

Figure 2. Comparison of amplitude and phase-detection imaging of blends with bulk compositions of 40% PSA/60% PLA (scale as shown in Figure 1): (a) Amplitude-detection imaging of 40% PSA/60% PLA. Height changes 37 nm. (b) Phase-detection imaging of 40% PSA/60% PLA. Maximum phase shift 52°.

this sample is shown in Figure 2. The amplitude-detection data in Figure 2a show the topography of a region of the blend surface. Spherulitic organization is evident on this surface, and this can again be attributed to the PSA component. However, the fibrous organization of the spherulites is not as clearly defined as on the data from the 60% PSA/40% PLA, and this appears to be caused by a partial coverage of the PSA by a second-component overlayer. This overlayer is clearly visualized in the phase-detection imaging AFM data, and again this overlayer generates a positive phase shift (for this image the shift was +52°). Comparing Figure 2b and 1b, it is evident that the surface coverage of the overlayer material increased as the amount of PLA in the original blend formula increased. This increased surface coverage is in agreement with XPS studies[12] and, therefore, strongly suggests that the overlayer is PLA.

Many authors have noted alternative contrast mechanisms in phase-detection imaging and that the unequivocal assignment of the cause of phase contrast on a particular sample can be problematic due to the number of acquisition and material variables involved (17, 25, 28, and 29). Here, we investigate the phase-

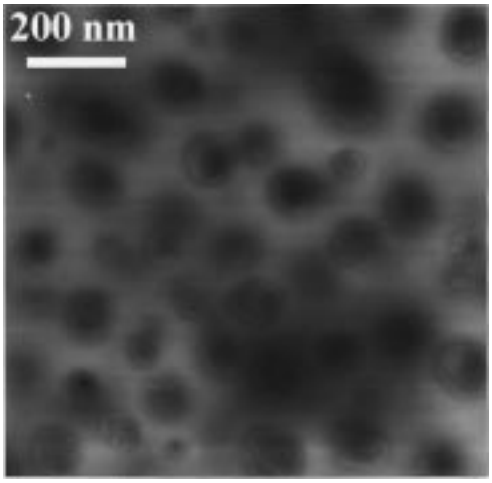

Figure 3. Amplitude-detection image of a 50% PSA/50% PLA blend confirming the presence of PSA microdomains in a network of PLA. Maximum height change 43 nm.

contrast mechanism on the PSA−PLA system involved when soft and moderate tapping are employed. The phase separation of the PSA/PLA blend provides an excellent sample on which to study the image contrast mode further. Contrast mechanisms have been investigated by recording phase-distance and amplitude-distance curves on the PSA and PLA components and by comparing the forward and reverse traces of the AFM data. This comparison has been performed on a 60% PSA/40% PLA blend sample prepared on a glass substrate. This sample displays a prominent phase separation in which the PLA component forms a network around PSA microdomains. This phase-separated morphology is evident in topographical data as shown in Figure 3.

Amplitude- and phase-distance curves recorded on the PSA and PLA portions of the blend surface are shown in Figure 4a. The soft and moderate setpoints are also indicated in Figure 4a. A number of points can be made from these data. First, at the soft setpoint the phase shifts on PSA and PLA are almost identical; hence, little phase contrast should be evident, while under moderate tapping conditions, there is a significant difference in the phase shifts on the two polymers, with the larger shift being observed on the PLA. Second, the amplitude curves which nominally should decay monotonically as the probe approaches the surfaces have a plateau region between the two chosen setpoints. This, we believe, reflects a transition region from where attractive forces on the cantilever dominate to where repulsive forces dominate. During this transition the phase curves display an inflection from a negative to a positive gradient. Such an inflection has been shown by Krüger et al.[27,30] to be indicative of the onset of repulsive interactions. Finally, once a difference in phase shift between the PSA and PLA becomes apparent, the PLA always shows the greater shift, at least up to the highest amplitude reduction value of 72% ($A_s/A_0 = 0.28$) that we employed in our experiments. Hence, no contrast reversal between the PSA and PLA in the phase data is observed with increasing hardness of tapping. This differs from phase contrast reversal which has been observed on polyurethane blends.[27]

Forward and reverse traces were recorded across one PSA microdomain (see Figure 4b−d)). The forward and reverse traces of the topography are in close agreement with each other (Figure 4b), and this is true whether

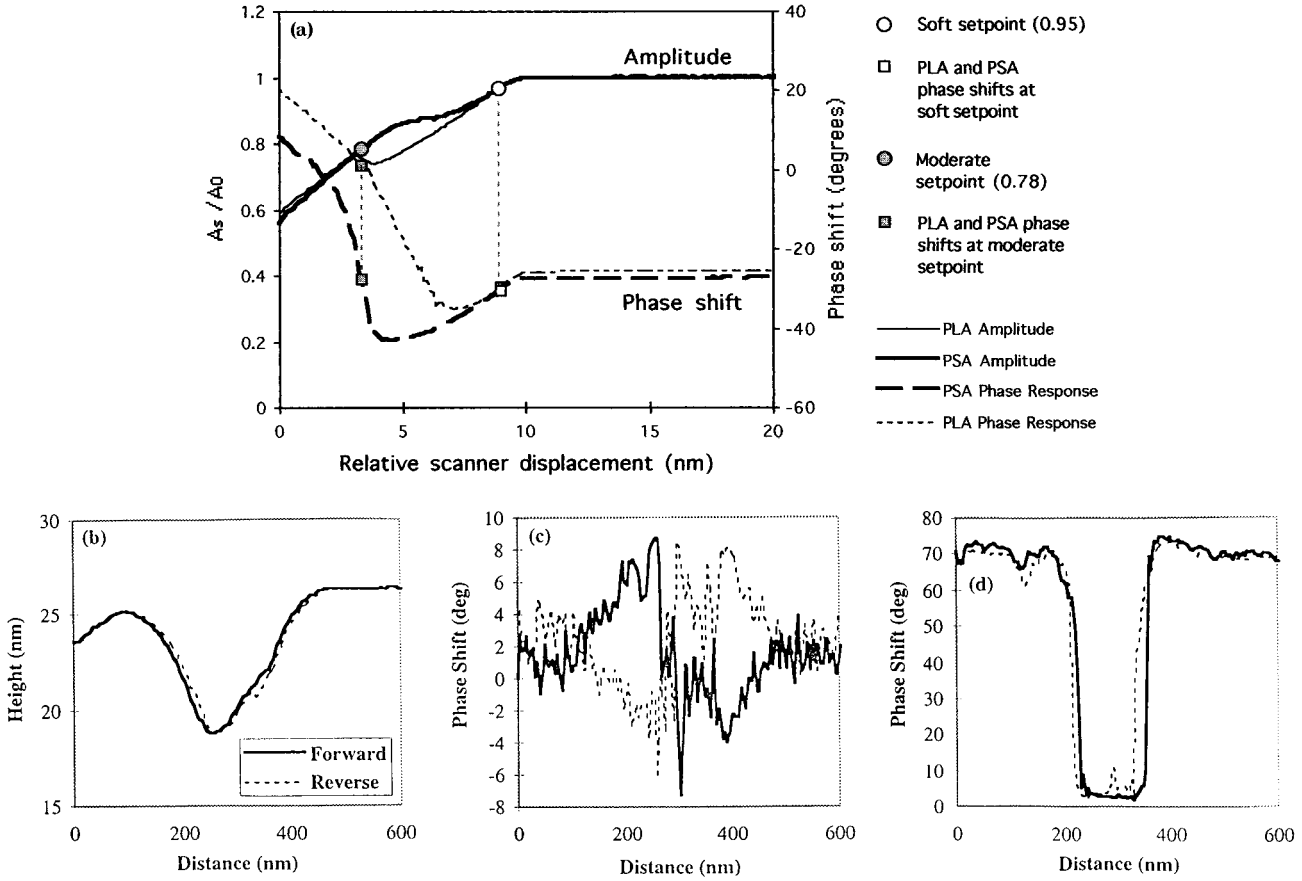

Figure 4. (a) Cantilever vibration amplitude and phase shift measured on 60% PSA and 40% PLA blend. Curves represent averages of four locations each on the PSA and PLA. Data are acquired as the probe approaches the surface vibrated at 323 kHz with a drive voltage of 45 mV. At the soft setpoint ($A_s/A_0 = 0.95$) the phase shifts on PSA and PLA are almost identical; hence, little phase contrast should be evident, while under moderate tapping conditions ($A_s/A_0 = 0.78$) there is a significant difference in the phase shifts on the two polymers, with the larger shift being observed on the PLA. (b–d) Forward (bold) and reverse traces (light) recorded across a PSA microdomain. In (b) the forward and reverse traces of the topography are in close agreement with each other and this is true whether soft or moderate tapping is employed (soft tapping shown). Both foward and reverse traces show a pit, which marks the PSA microdomain, surrounded by the PLA network. (c) With soft tapping, the phase data of the forward and reverse traces were mirror images of each other. (d) Simultaneously recorded moderate tapping traces display phase shifts of about 70° across all of the surface of the pit. Here, the forward and reverse traces are in close agreement.

soft or moderate tapping is employed (soft tapping shown). Both traces show a pit, which marks a PSA microdomain, surrounded by the PLA network. With soft tapping (i.e., when there is no significant phase-shift difference between the PSA and PLA) the phase data of the forward and reverse traces were mirror images of each other (Figure 4c). Following the forward trace from left to right, one can see that when the topographical trace sloped downward, forming the front edge of the pit, there was a small positive phase shift of about 8°. This phase shift was reversed when the topography slopes upward at the back edge of the pit. The reverse trace is a mirror image because downward slopes on the forward trace are now encountered as upward slopes and vice versa. Therefore, the image contrast of the phase data during soft tapping is generated by changes in the surface topography. However, while amplitude-detection imaging records the actual height of features, phase-detection imaging with soft tapping records the changes in the gradient of the topography.

In the data recorded using moderate tapping, the forward and reverse traces display phase shifts of up to 70° across all of the surface of the pit (Figure 4d). In addition, the forward and reverse traces are in close agreement. The magnitude of the phase shift and the agreement of forward and reverse traces indicate that the dominant image contrast mechanism is the nature of the interaction between the polymer surface and the AFM probe (as also indicated by Figure 4a), controlled by polymer stiffness, viscoelasticity, or adhesion, not topographical variations.

Therefore, when tapping softly on the polymer surface, the phase-detection image generates a representation of gradient changes across the sample surface. When the strength of tapping is increased, these gradient changes are masked by the much larger phase changes induced by variations in viscoelasticity, stiffness, or adhesion between the PSA and PLA regions of the surface.

The benefits of employing phase-detection imaging to analyze polymer surfaces are not limited to the investigation of multicomponent surfaces. The contrast mechanism involved in phase-detection imaging appears to make the technique valuable in the study of lamellar organization at spherulite surfaces. The high contrast and resolution achieved during the imaging of polymer lamellae is demonstrated by the images in Figure 5. These images were recorded on the PSA surfaces. The lamellar organization of the spherulites on the nanometer-length scale is very clear in the phase-detection images. In addition, it is apparent that the phase-

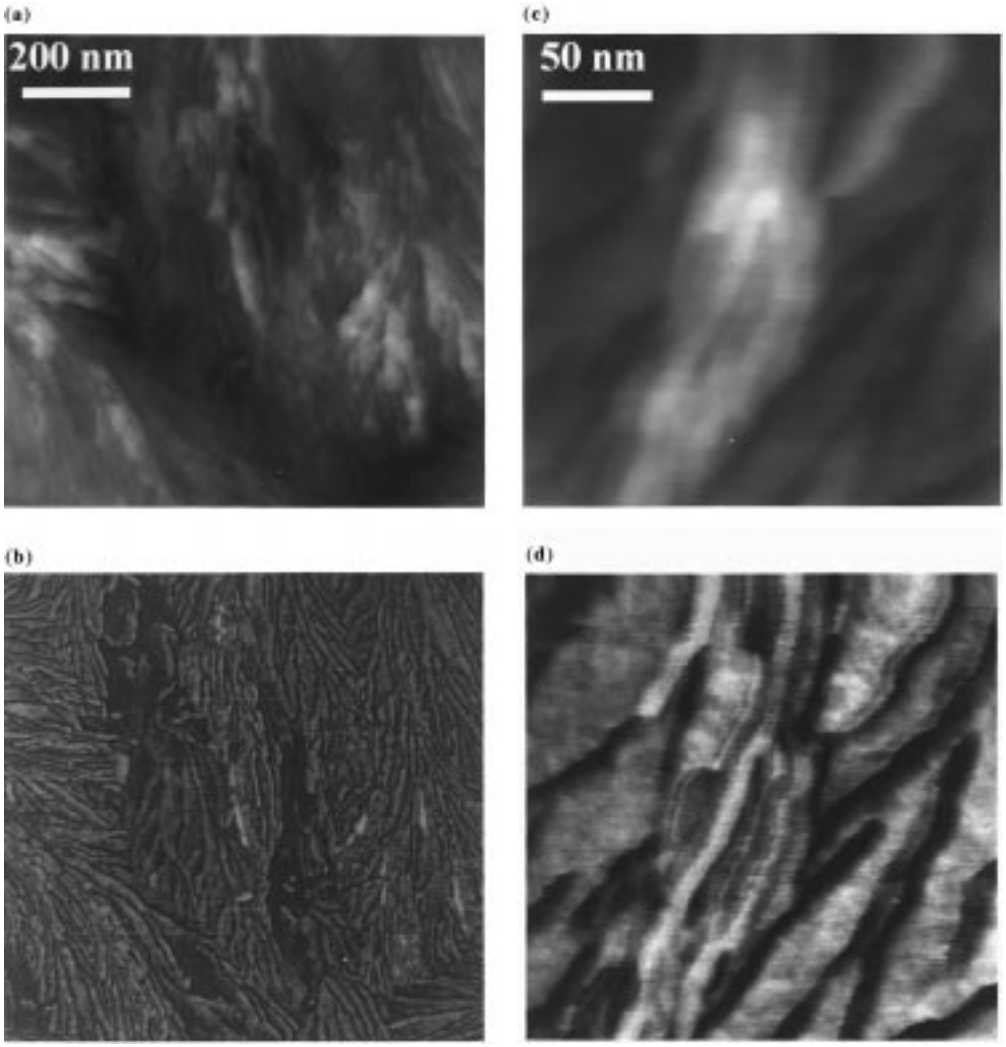

Figure 5. Comparison of topographical and phase-detection images of PSA spherulites and lamellae: (a) Amplitude-detection imaging with height variation of 34 nm. (b) Phase-detection imaging with maximum phase shift 31°. (c) Amplitude-detection imaging with height variation of 12 nm. (d) Phase-detection imaging with maximum phase shift 27°.

detection image has resolved lamellae with widths of less than 5 nm. These lamellae cannot be resolved on the topographical data.

The phase-detection images of the PSA lamellae bear some similarity to electron microscopy images of spherulite surfaces after these surface have been etched to remove amorphous material.[31] These etching procedures were developed to allow crystalline lamellae to be resolved. It is possible that moderate tapping during phase imaging has a similar effect to surface etching because crystalline lamellae make a larger contribution to the phase data than amorphous regions.

Conclusions

The differentiation of polymer components at the surfaces of blends by phase-detection imaging AFM provides a powerful technique for assessing surface enrichment phenomenon. The ability to detect the presence and structure of PLA domains on the blend surfaces provides further evidence of the potential to use this imaging technique to characterize complex surfaces. In the case of biodegradable polymer blends, knowledge of this surface organization can be used to predict the behavior of fabricated biomaterials. Because of the surface enrichment of the PLA component in PLA/PSA blends, it can be predicted that initial surface erosion kinetics will be strongly influenced by the PLA material, and therefore, surface erosion will occur at a slower rate than predicted from the bulk composition of the blends. The novelty of the surface information derived is that it establishes the relationship between PLA microdomain organization and the overall surface chemistry of the blend films.

We have also contributed to the debate on the complex image mechanisms involved in phase data. In particular, we have shown that when tapping softly on the polymer surface, the phase-detection image generates a representation of gradient changes across the sample surface and that when the strength of tapping is increased, these gradients changes are masked by the much larger phase changes induced by variations in surface mechanical properties. Also, by recording amplitude and phase-distance curves, we have identified the transition region from attractive forces dominating the response of the cantilever to repulsive forces dominating.

Acknowledgment. The authors thank Mike Allen of Digital Instruments and Nicola Forsyth of LOT Oriel for their excellent support. X.C. acknowledges the support of the BBSRC and Ortho Clinical Diagnostics. S.L.M. thanks the BBSRC for providing his studentship.

S.J.B.T. is a Nuffield Foundation Science Research Fellow.

References and Notes

(1) Elbert, D. L.; Hubbell, J. A. *Annu. Rev. Mater. Sci.* **1996**, *26*, 365.
(2) Hubbell, J. A. *Biotechnology* **1995**, *13*, 565.
(3) Ratner, B. D. *J. Mol. Recognit.* **1996**, *9*, 617.
(4) Cook, A. D.; Hrkach, J. S.; Gao, N. N.; Johnson, I. M.; Pajvani, U. B.; Cannizzaro, S. M.; Langer, R. *J. Biomed. Mater. Res.* **1997**, *35*, 513.
(5) Hrkach, J. S.; Ou, J.; Lotan, N.; Langer, R. *Macromolecules* **1995**, *28*, 4736.
(6) Chen, X.; Gardella, J. A. *Macromolecules* **1994**, *27*, 3363.
(7) Su, Z.; Wu, D.; Hsu, S. L.; McCarthy, T. J. *Macromolecules* **1997**, *30*, 840.
(8) Yoon, S. C.; Ratner, B. D.; Iván, B.; Kennedy, J. P. *Macromolecules* **1994**, *27*, 1548.
(9) Shakesheff, K. M.; Evora, C.; Soriano, I.; Langer, R. *J. Colloid Interface Sci.* **1996**, *185*, 538.
(10) Bletsos, I. V.; Hercules, D. M.; vanLeyen, D.; Benninghoven, A. *Macromolecules* **1987**, *20*, 407.
(11) Hearn, M. J.; Ratner, B. D.; Brigg, D. *Macromolecules* **1988**, *21*, 2950.
(12) Davies, M. C.; Shakesheff, K. M.; Shard, A. G.; Domb, A.; Roberts, C. J.; Tendler, S. J. B.; Williams, P. M. *Macromolecules* **1996**, *29*, 2205.
(13) Domb, A. J. *J. Polym. Sci., Part A: Polym. Chem.* **1993**, *31*, 1973.
(14) Shakesheff, K. M.; Chen, X. Y.; Davies, M. C.; Domb, A.; Roberts, C. J.; Tendler, S. J. B.; Williams, P. M. *Langmuir* **1995**, *11*, 3921.
(15) Akari, S. O.; van der Vegte, E. W.; Grim, P. C. M.; Belder, G. F.; Koutsos, V.; ten Brinke, G.; Hadziioannou, G. *Appl. Phys. Lett.* **1994**, *65*, 1915.
(16) Schmitz, I.; Schreiner, M.; Friedbacher, G.; Grasserbauer, M. *Appl. Surf. Sci.* **1997**, *115*, 190.
(17) Magonov, S. N.; Elings, V.; Whangbo, M. H. *Surf. Sci.* **1997**, *375*, L385.
(18) Kajiyama, T.; Ohki, I.; Tanaka, K.; Ge, S. R.; Takahara, A. *Proc. Jpn. Acad. Ser. B: Phys. Biol. Sci.* **1995**, *71*, 75.
(19) Kajiyama, T.; Tanaka, K.; Ohki, I.; Ge, S. R.; Yoon, J. S.; Takahara, A. *Macromolecules* **1994**, *27*, 7932.
(20) Viswanathan, R.; Tian, J.; Marr, D. W. M. *Langmuir* **1997**, *13*, 1840.
(21) Leclere, P.; Lazzaroni, R.; Bredas, J. L.; Yu, J. M.; Dubois, P.; Jerome, R. *Langmuir* **1996**, *12*, 4317.
(22) Akari, S. O.; Vandervegte, E. W.; Grim, P. C. M.; Belder, G. F.; Koutsos, V.; Tenbrinke, G.; Hadziioannou, G. *Appl. Phys. Lett.* **1994**, *65*, 1915.
(23) Keita, B.; Nadjo, L.; Gachard, E.; Remita, H. *New J. Chem.* **1997**, *21*, 851.
(24) Domb, A. J.; Amselem, S.; Shah, J.; Maniar, M. *Adv. Polym. Sci.* **1993**, *107*, 93.
(25) Schmitz, I.; Schreiner, M.; Friedbacher, G.; Grasserbauer, M. *Appl. Surf. Sci.* **1997**, *115*, 190.
(26) Tamayo, A.; Garcia, R. *Langmuir* **1996**, *12*, 4430.
(27) Krüger, D.; Anczykowski, B.; Fuchs, H. *Ann. Phys.* **1997**, *6*, 341.
(28) Burnham, N. A.; Behrend, O. P.; Oulevey, F.; Gremaud, G.; Gallo, P. J.; Gourdon, D.; Dupas, E.; Kulik, A. J.; Pollock, H. M.; Briggs_GAD, *Nanotechnology* **1997**, *8*, 67.
(29) VanNoort, S. J. T.; VanderWerf, K. O.; DeGrooth, B. G.; VanHulst, N. F.; Greve, J. *Ultramicroscopy* **1997**, *69*, 117.
(30) Anczykowski, B.; Kruger, D.; Babcock, K. L.; Fuchs, H. *Ultramicroscopy* **1996**, *66*, 251.
(31) Bassett, D. C. *CRC Crit. Rev. Solid State Mater. Sci.* **1984**, *12*, 97−165.

MA9704525